The Dijet Mass Spectrum at DØ

The DØ Collaboration *
Fermi National Accelerator Laboratory, Batavia, Illinois 60510
(July 18, 1997)

Abstract

We present preliminary results from an analysis of jet data collected during the 1994-95 Tevatron Collider run with an integrated luminosity of 93 pb^{-1} . Measurements of dijet mass spectra in $\overline{p}p$ collisions at $\sqrt{s} = 1.8$ TeV are compared to next-to-leading order QCD calculations.

---

*Submitted to the *XVIII International Symposium on Lepton Photon Interactions,* July 28 – August 1, 1997, Hamburg, Germany.

B. Abbott,[28] M. Abolins,[25] B.S. Acharya,[43] I. Adam,[12] D.L. Adams,[37] M. Adams,[17] S. Ahn,[14] H. Aihara,[22] G.A. Alves,[10] E. Amidi,[29] N. Amos,[24] E.W. Anderson,[19] R. Astur,[42] M.M. Baarmand,[42] A. Baden,[23] V. Balamurali,[32] J. Balderston,[16] B. Baldin,[14] S. Banerjee,[43] J. Bantly,[5] J.F. Bartlett,[14] K. Bazizi,[39] A. Belyaev,[26] S.B. Beri,[34] I. Bertram,[31] V.A. Bezzubov,[35] P.C. Bhat,[14] V. Bhatnagar,[34] M. Bhattacharjee,[13] N. Biswas,[32] G. Blazey,[30] S. Blessing,[15] P. Bloom,[7] A. Boehnlein,[14] N.I. Bojko,[35] F. Borcherding,[14] C. Boswell,[9] A. Brandt,[14] R. Brock,[25] A. Bross,[14] D. Buchholz,[31] V.S. Burtovoi,[35] J.M. Butler,[3] W. Carvalho,[10] D. Casey,[39] Z. Casilum,[42] H. Castilla-Valdez,[11] D. Chakraborty,[42] S.-M. Chang,[29] S.V. Chekulaev,[35] L.-P. Chen,[22] W. Chen,[42] S. Choi,[41] S. Chopra,[24] B.C. Choudhary,[9] J.H. Christenson,[14] M. Chung,[17] D. Claes,[27] A.R. Clark,[22] W.G. Cobau,[23] J. Cochran,[9] W.E. Cooper,[14] C. Cretsinger,[39] D. Cullen-Vidal,[5] M.A.C. Cummings,[16] D. Cutts,[5] O.I. Dahl,[22] K. Davis,[2] K. De,[44] K. Del Signore,[24] M. Demarteau,[14] D. Denisov,[14] S.P. Denisov,[35] H.T. Diehl,[14] M. Diesburg,[14] G. Di Loreto,[25] P. Draper,[44] Y. Ducros,[40] L.V. Dudko,[26] S.R. Dugad,[43] D. Edmunds,[25] J. Ellison,[9] V.D. Elvira,[42] R. Engelmann,[42] S. Eno,[23] G. Eppley,[37] P. Ermolov,[26] O.V. Eroshin,[35] V.N. Evdokimov,[35] T. Fahland,[8] M. Fatyga,[4] M.K. Fatyga,[39] J. Featherly,[4] S. Feher,[14] D. Fein,[2] T. Ferbel,[39] G. Finocchiaro,[42] H.E. Fisk,[14] Y. Fisyak,[7] E. Flattum,[14] G.E. Forden,[2] M. Fortner,[30] K.C. Frame,[25] S. Fuess,[14] E. Gallas,[44] A.N. Galyaev,[35] P. Gartung,[9] T.L. Geld,[25] R.J. Genik II,[25] K. Genser,[14] C.E. Gerber,[14] B. Gibbard,[4] S. Glenn,[7] B. Gobbi,[31] M. Goforth,[15] A. Goldschmidt,[22] B. Gómez,[1] G. Gómez,[23] P.I. Goncharov,[35] J.L. González Solís,[11] H. Gordon,[4] L.T. Goss,[45] K. Gounder,[9] A. Goussiou,[42] N. Graf,[4] P.D. Grannis,[42] D.R. Green,[14] J. Green,[30] H. Greenlee,[14] G. Grim,[7] S. Grinstein,[6] N. Grossman,[14] P. Grudberg,[22] S. Grünendahl,[39] G. Guglielmo,[33] J.A. Guida,[2] J.M. Guida,[5] A. Gupta,[43] S.N. Gurzhiev,[35] P. Gutierrez,[33] Y.E. Gutnikov,[35] N.J. Hadley,[23] H. Haggerty,[14] S. Hagopian,[15] V. Hagopian,[15] K.S. Hahn,[39] R.E. Hall,[8] P. Hanlet,[29] S. Hansen,[14] J.M. Hauptman,[19] D. Hedin,[30] A.P. Heinson,[9] U. Heintz,[14] R. Hernández-Montoya,[11] T. Heuring,[15] R. Hirosky,[15] J.D. Hobbs,[14] B. Hoeneisen,[1,†] J.S. Hoftun,[5] F. Hsieh,[24] Ting Hu,[42] Tong Hu,[18] T. Huehn,[9] A.S. Ito,[14] E. James,[2] J. Jaques,[32] S.A. Jerger,[25] R. Jesik,[18] J.Z.-Y. Jiang,[42] T. Joffe-Minor,[31] K. Johns,[2] M. Johnson,[14] A. Jonckheere,[14] M. Jones,[16] H. Jöstlein,[14] S.Y. Jun,[31] C.K. Jung,[42] S. Kahn,[4] G. Kalbfleisch,[33] J.S. Kang,[20] R. Kehoe,[32] M.L. Kelly,[32] C.L. Kim,[20] S.K. Kim,[41] A. Klatchko,[15] B. Klima,[14] C. Klopfenstein,[7] V.I. Klyukhin,[35] V.I. Kochetkov,[35] J.M. Kohli,[34] D. Koltick,[36] A.V. Kostritskiy,[35] J. Kotcher,[4] A.V. Kotwal,[12] J. Kourlas,[28] A.V. Kozelov,[35] E.A. Kozlovski,[35] J. Krane,[27] M.R. Krishnaswamy,[43] S. Krzywdzinski,[14] S. Kunori,[23] S. Lami,[42] H. Lan,[14,*] R. Lander,[7] F. Landry,[25] G. Landsberg,[14] B. Lauer,[19] A. Leflat,[26] H. Li,[42] J. Li,[44] Q.Z. Li-Demarteau,[14] J.G.R. Lima,[38] D. Lincoln,[24] S.L. Linn,[15] J. Linnemann,[25] R. Lipton,[14] Q. Liu,[14,*] Y.C. Liu,[31] F. Lobkowicz,[39] S.C. Loken,[22] S. Lökös,[42] L. Lueking,[14] A.L. Lyon,[23] A.K.A. Maciel,[10] R.J. Madaras,[22] R. Madden,[15] L. Magaña-Mendoza,[11] S. Mani,[7] H.S. Mao,[14,*] R. Markeloff,[30] T. Marshall,[18] M.I. Martin,[14] K.M. Mauritz,[19] B. May,[31] A.A. Mayorov,[35] R. McCarthy,[42] J. McDonald,[15] T. McKibben,[17] J. McKinley,[25] T. McMahon,[33] H.L. Melanson,[14] M. Merkin,[26] K.W. Merritt,[14] H. Miettinen,[37] A. Mincer,[28] C.S. Mishra,[14] N. Mokhov,[14] N.K. Mondal,[43] H.E. Montgomery,[14] P. Mooney,[1] H. da Motta,[10] C. Murphy,[17] F. Nang,[2] M. Narain,[14] V.S. Narasimham,[43] A. Narayanan,[2] H.A. Neal,[24] J.P. Negret,[1] P. Nemethy,[28] M. Nicola,[10] D. Norman,[45]

L. Oesch,[24] V. Oguri,[38] E. Oltman,[22] N. Oshima,[14] D. Owen,[25] P. Padley,[37] M. Pang,[19]
A. Para,[14] Y.M. Park,[21] R. Partridge,[5] N. Parua,[43] M. Paterno,[39] J. Perkins,[44] M. Peters,[16]
R. Piegaia,[6] H. Piekarz,[15] Y. Pischalnikov,[36] V.M. Podstavkov,[35] B.G. Pope,[25]
H.B. Prosper,[15] S. Protopopescu,[4] J. Qian,[24] P.Z. Quintas,[14] R. Raja,[14] S. Rajagopalan,[4]
O. Ramirez,[17] L. Rasmussen,[42] S. Reucroft,[29] M. Rijssenbeek,[42] T. Rockwell,[25] N.A. Roe,[22]
P. Rubinov,[31] R. Ruchti,[32] J. Rutherfoord,[2] A. Sánchez-Hernández,[11] A. Santoro,[10]
L. Sawyer,[44] R.D. Schamberger,[42] H. Schellman,[31] J. Sculli,[28] E. Shabalina,[26] C. Shaffer,[15]
H.C. Shankar,[43] R.K. Shivpuri,[13] M. Shupe,[2] H. Singh,[9] J.B. Singh,[34] V. Sirotenko,[30]
W. Smart,[14] R.P. Smith,[14] R. Snihur,[31] G.R. Snow,[27] J. Snow,[33] S. Snyder,[4] J. Solomon,[17]
P.M. Sood,[34] M. Sosebee,[44] N. Sotnikova,[26] M. Souza,[10] A.L. Spadafora,[22]
R.W. Stephens,[44] M.L. Stevenson,[22] D. Stewart,[24] F. Stichelbaut,[42] D.A. Stoianova,[35]
D. Stoker,[8] M. Strauss,[33] K. Streets,[28] M. Strovink,[22] A. Sznajder,[10] P. Tamburello,[23]
J. Tarazi,[8] M. Tartaglia,[14] T.L.T. Thomas,[31] J. Thompson,[23] T.G. Trippe,[22] P.M. Tuts,[12]
N. Varelas,[25] E.W. Varnes,[22] D. Vititoe,[2] A.A. Volkov,[35] A.P. Vorobiev,[35] H.D. Wahl,[15]
G. Wang,[15] J. Warchol,[32] G. Watts,[5] M. Wayne,[32] H. Weerts,[25] A. White,[44] J.T. White,[45]
J.A. Wightman,[19] S. Willis,[30] S.J. Wimpenny,[9] J.V.D. Wirjawan,[45] J. Womersley,[14]
E. Won,[39] D.R. Wood,[29] H. Xu,[5] R. Yamada,[14] P. Yamin,[4] C. Yanagisawa,[42] J. Yang,[28]
T. Yasuda,[29] P. Yepes,[37] C. Yoshikawa,[16] S. Youssef,[15] J. Yu,[14] Y. Yu,[41] Z.H. Zhu,[39]
D. Zieminska,[18] A. Zieminski,[18] E.G. Zverev,[26] and A. Zylberstejn[40]

(DØ Collaboration)

[1]Universidad de los Andes, Bogotá, Colombia
[2]University of Arizona, Tucson, Arizona 85721
[3]Boston University, Boston, Massachusetts 02215
[4]Brookhaven National Laboratory, Upton, New York 11973
[5]Brown University, Providence, Rhode Island 02912
[6]Universidad de Buenos Aires, Buenos Aires, Argentina
[7]University of California, Davis, California 95616
[8]University of California, Irvine, California 92697
[9]University of California, Riverside, California 92521
[10]LAFEX, Centro Brasileiro de Pesquisas Físicas, Rio de Janeiro, Brazil
[11]CINVESTAV, Mexico City, Mexico
[12]Columbia University, New York, New York 10027
[13]Delhi University, Delhi, India 110007
[14]Fermi National Accelerator Laboratory, Batavia, Illinois 60510
[15]Florida State University, Tallahassee, Florida 32306
[16]University of Hawaii, Honolulu, Hawaii 96822
[17]University of Illinois at Chicago, Chicago, Illinois 60607
[18]Indiana University, Bloomington, Indiana 47405
[19]Iowa State University, Ames, Iowa 50011
[20]Korea University, Seoul, Korea
[21]Kyungsung University, Pusan, Korea
[22]Lawrence Berkeley National Laboratory and University of California, Berkeley, California 94720
[23]University of Maryland, College Park, Maryland 20742
[24]University of Michigan, Ann Arbor, Michigan 48109
[25]Michigan State University, East Lansing, Michigan 48824
[26]Moscow State University, Moscow, Russia
[27]University of Nebraska, Lincoln, Nebraska 68588
[28]New York University, New York, New York 10003
[29]Northeastern University, Boston, Massachusetts 02115
[30]Northern Illinois University, DeKalb, Illinois 60115
[31]Northwestern University, Evanston, Illinois 60208
[32]University of Notre Dame, Notre Dame, Indiana 46556
[33]University of Oklahoma, Norman, Oklahoma 73019
[34]University of Panjab, Chandigarh 16-00-14, India
[35]Institute for High Energy Physics, 142-284 Protvino, Russia
[36]Purdue University, West Lafayette, Indiana 47907
[37]Rice University, Houston, Texas 77005
[38]Universidade do Estado do Rio de Janeiro, Brazil
[39]University of Rochester, Rochester, New York 14627
[40]CEA, DAPNIA/Service de Physique des Particules, CE-SACLAY, Gif-sur-Yvette, France
[41]Seoul National University, Seoul, Korea
[42]State University of New York, Stony Brook, New York 11794
[43]Tata Institute of Fundamental Research, Colaba, Mumbai 400005, India
[44]University of Texas, Arlington, Texas 76019
[45]Texas A&M University, College Station, Texas 77843

I. INTRODUCTION

The production of hadronic jets is the dominant contribution to high transverse momentum (p_{T}) processes in proton–antiproton ($\overline{p}p$) collisions. High p_{T} jets have been observed since the early phase of experimentation at the CERN $\overline{p}p$ collider and their production properties are well described by perturbative Quantum Chromodynamics (QCD). Theoretical predictions for the inclusive jet cross section (and hence the inclusive dijet cross section) have been made using next–to–leading order (NLO) QCD [1–3]. These $\mathcal{O}({\alpha_s}^3)$ calculations, which include the possibility of a third radiated parton, reduce theoretical uncertainties to $\sim$30%. We measure the inclusive dijet mass spectrum in the DØ detector [4] at the Fermilab Tevatron Collider at $\sqrt{s} = 1.8$ TeV. Comparison of this measurement to NLO calculations tests QCD over five orders of magnitude.

II. JET AND EVENT SELECTION

Jet detection in the DØ detector makes primary use of the uranium–liquid argon calorimeters which cover pseudorapidity $|\eta| \leq 4$ ($\eta = -\ln(\tan(\theta/2))$ where θ is the polar angle relative to the proton beam). The calorimeters have electromagnetic and hadronic single particle resolutions of $15\%/\sqrt{E}$ (GeV) and $50\%/\sqrt{E}$ (GeV), respectively. They are transversely segmented into projective towers of $\Delta\eta \times \Delta\phi = 0.1 \times 0.1$, where ϕ is the azimuthal angle, and are divided longitudinally into eight to eleven segments depending on η. The electromagnetic modules (EM) include the first four longitudinal segments and the coarse hadronic modules (CH) the final longitudinal segment. The intervening segments comprise the fine hadronic modules and the intercryostat detectors. The total calorimetric depth exceeds seven nuclear interaction lengths for $|\eta| \leq 0.5$. The calorimeters are also segmented into trigger tiles of $\Delta\eta \times \Delta\phi = 0.8 \times 1.6$ and trigger towers of $\Delta\eta \times \Delta\phi = 0.2 \times 0.2$. The event vertex is determined using tracks reconstructed in the central tracking system. The detector includes two trigger scintillator hodoscopes located on each side of the interaction region at $1.9 < |\eta| < 4.3$. Timing distributions of particles traversing the two hodoscopes indicate the occurrence of a single inelastic interaction or of multiple inelastic interactions during a single beam–beam crossing.

Event selection occurred in two hardware stages and a final software stage. The initial hardware trigger selected an inelastic particle collision as indicated by the hodoscopes. The next trigger stage required transverse energy above a preset threshold in the calorimeter trigger tiles. Selected events were then digitized and sent to an array of processors. Jet candidates were then reconstructed with a fast cone algorithm and the event logged to tape if any jet E_{T} exceeded a specified threshold. During the 1994–1995 data run, the software jet thresholds were 30, 50, 85, and 115 GeV with integrated luminosities of 0.366 ± 0.020, 4.76 ± 0.13, 56.0 ± 3.4 and 93.0 ± 6.1 pb^{-1} respectively. To avoid saturating the data acquisition bandwidth, only a fraction of the lower threshold triggers were accepted.

Jets are reconstructed offline using an iterative jet cone algorithm with a cone radius of $\mathcal{R}$=0.7 in η–ϕ space [5]. The algorithm uses preclusters formed from 1 GeV seed towers.

The jet E_{T} is defined as the sum of each cell E_{T} within the cone. The E_{T} –weighted rapidity and azimuth of the jet are calculated and the cone is centered on this axis. The jet E_{T} and direction are then recalculated until the cone direction is stable. The final jet directions are calculated using the components of the jet energy vector. If two jets share energy, they are combined or split, based on the fraction of energy shared relative to the E_{T} of the lower E_{T} jet. If the shared fraction exceeds 50% the jets are combined and the directions accordingly recalculated. For the 1994–1995 data, prior to reconstruction, isolated energetic cells (mainly due to calorimeter noise) were removed from the event. This occurred for 3% of 100 GeV jets and for 10% of 350 GeV jets. In some cases this procedure removed energy that was not due to noise. To correct this, any removed cell located within $\mathcal{R}$=0.7 of a jet axis was restored to the jet if all of the restored cells had no more than 50% of the final restored jet energy. The restored jet rapidity was recalculated using the E_{T} weighted rapidity of the jet and restored cell.

Background jets from isolated noisy calorimeter cells and accelerator losses were eliminated with quality cuts. The fraction of energy detected in the EM modules for any jet must be between 5% and 95%. Also the ratio of energy in the second most energetic cell in a jet to the most energetic cell must be greater than 0.10 (this cut is not imposed on jets which include restored cells). Background from the Main Ring accelerator passing through the CH modules is eliminated by requiring that the fraction of the jet energy in the CH modules be less than 40%. It is required that the two leading E_{T} jets pass these quality cuts for the event to be accepted. Background from cosmic ray bremsstrahlung is eliminated by requiring the magnitude of the summed transverse energy in an event, $|\not{E}_T|$, be less than 70% of the leading jet E_{T}. Residual contamination from the backgrounds is estimated to be less than 2% at all $E_{\mathrm{T}} < 500$ GeV based on Monte-Carlo simulations and scanning of all very high jet E_{T} candidates [6]. The overall jet selection efficiency for $|\eta| \leq 0.5$ has been measured as a function of jet E_{T} and found to be $97 \pm 1\%$ below 250 GeV and $94 \pm 1\%$ at 400 GeV.

At high instantaneous luminosity more than one interaction in a single beam crossing is probable. The event reconstruction retains, at most, two vertices. The quantity $\mathcal{H}_T = |\Sigma_{\mathrm{jets}} \vec{E_{\mathrm{T}}}^{\mathrm{jet}}|$ was calculated for both vertices. The vertex with the minimum $\mathcal{H}_T$ was selected as the event vertex and used to calculate jet E_{T} and η. The selected vertex was also required to be within 50 cm of the detector center. The event vertex requirement is $90 \pm 1\%$ efficient, independent of E_{T}.

III. ENERGY CALIBRATION

The transverse energy of each jet has been corrected for an offset, O, due to underlying event, multiple $\overline{p}p$ interactions pileup and noise; the fraction of particle energy showering, S, outside the jet cone; and calorimeter hadronic energy response, R. The corrected jet energy, E_{jet}, can be related to the measured jet energy, E_{meas}, by $E_{\mathrm{jet}} = [E_{\mathrm{meas}} - O]/[(1-S) \times R]$. The offset to the jet energy were extracted from the energy densities as a function of η using minimum bias events at low luminosity and zero bias events at high luminsoity. The underlying interaction correction for each jet is determined using the instantaneous luminosity observed at the time the jet was recorded.

The out–of–cone showering correction compensates for energy (from particles emitted within the cone) that leaks outside the cone during calorimeter showering. This puts the experimental measure of jet energy on an identical footing to the theoretical NLO treatment which includes parton radiation inside the cone. Similarly, S must compensate for particles emitted outside the cone but which shower some energy inside.

The absolute energy calibration of the electromagnetic calorimeter is determined using dielectron and diphoton decays of the Z [8], J/ψ, and π^0 resonances. The response of the calorimeter to electrons is linear to $\leq 1\%$ for energies above 10 GeV [7]. The response of the calorimeter relative to the electromagnetic calibration, the hadronic response correction is based on the $\not{E}_T$ balance in a photon–jets event sample. The photon candidates, designated "γ", include direct photons and jets with a high π^0 /η fraction that have fragmented into photons. The "γ" candidates were selected by requiring a reconstructed electromagnetic deposition, candidate isolation, and shower shape consistent with that of a test beam electron [7]. The latter two requirements ensure that these "γ" candidates have electromagnetic response similar to the events used in the electromagnetic calibration. The hadronic response for "γ" events can be derived from data using the conservation of momentum: $R = 1 + [\hat{n_{T\gamma}} \cdot \vec{\not{E}_T}]/E_{T\gamma}$, where $\hat{n_{T\gamma}}$ and $E_{T\gamma}$ are the transverse direction vector and energy of the γ and $\vec{\not{E}_T}$ is the missing E_{T} vector. Figure 1 shows the measured hadronic response as a function of the uncorrected jet energy.

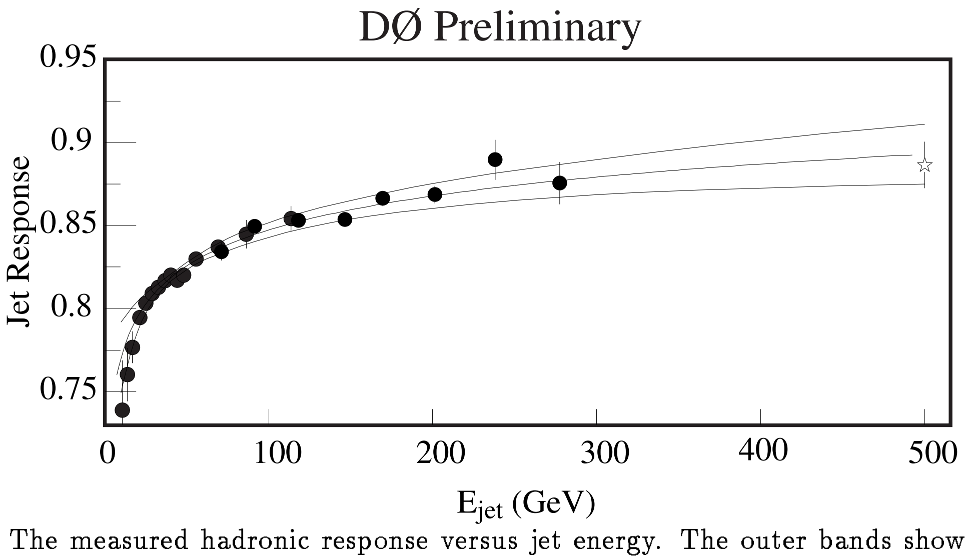

FIG. 1. The measured hadronic response versus jet energy. The outer bands show the limits of the measured response for high energy jets at the 68% confidence level. The solid circles show the measured data and the open star shows a MC generated data point.

IV. RESOLUTION UNSMEARING

The jet energy scale corrects only the average response of a jet. The steeply falling dijet mass spectrum is distorted by jet energy resolution and to a negligible extent by the η resolution. The observed mass spectrum is corrected for resolution smearing by assuming a trial unsmeared spectrum

$$F(M') = A \cdot M'^{-\alpha} \left(1 - \frac{M'}{\sqrt{S}}\right)^{-\beta} \tag{1}$$

which is convoluted with the mass resolutions to obtain the smeared spectrum:

$$f(M) = \int F(M')\sigma(M' - M, M')\, dM' \tag{2}$$

Hence the number of events in any mass bin is given by:

$$F_i = \int_{M_{\rm min}}^{M_{\rm max}} f(M) dM \tag{3}$$

The data are fitted using a binned maximum likelihood to determine the values of A, α and β. The unsmearing correction for each mass bin is then given by the ratio:

$$\frac{\int_{M_{\rm min}}^{M_{\rm max}} F(M) dM}{F_i} \tag{4}$$

The mass resolutions were calculated using the measured single jet resolutions [6]. The mass resolution depends on the $E_{\rm T}$ and η distribution of the two leading $E_{\rm T}$ jets in each event. Hence, the resolution is determined using a Monte Carlo event generator (PYTHIA [9]). For each event generated the individual particle jets (partons for the JETRAD program) are smeared by the measured single jet resolutions [6]. The unsmeared and smeared dijet masses are then calculated and used to determine the mass smearing ($M_{\rm smeared}/M_{\rm unsmeared}$).

Figure 2 shows the unsmearing correction as a function of mass. The magnitude of the correction is approximately 4% at 200 GeV/c^2 and drops to approximately 3% at 500 GeV/c^2 before rising to 8% at 1 TeV/c^2.

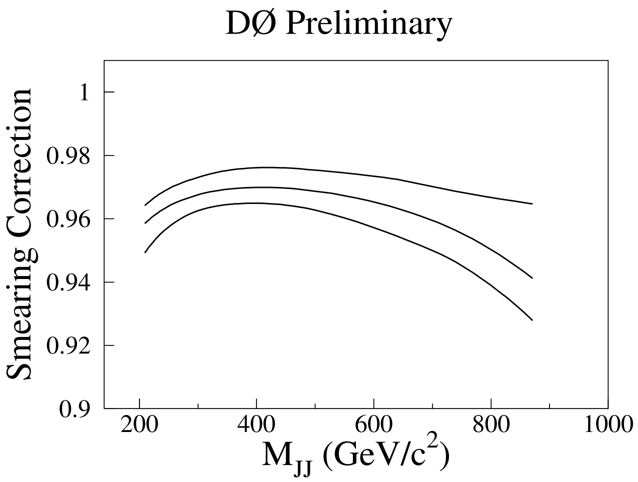

FIG. 2. The smearing correction applied to the data when the two highest E_{T} jets satisfy $|\eta| < 1.0$. The central curve shows the nominal unsmearing correction and the upper and lower curves show the $\pm$ 1 sigma systematic uncertainties on the correction.

V. INCLUSIVE DIJET MASS DISTRIBUTION

For each event that passes the quality cuts, the dijet mass can be calculated, assuming that the jets are massless: $M_{JJ}^2 = 2 \cdot E_{\mathrm{T}}{}^1 \cdot E_{\mathrm{T}}{}^2 \cdot (\cosh(\Delta\eta) - \cos(\Delta\phi))$. Each event is weighted by the reciprocal of the efficiency of the quality cuts applied to the data, w_i.

The inclusive dijet mass cross section is given by

$$\frac{\Delta d^2\sigma}{\Delta M_{\mathrm{JJ}} d\eta_1 d\eta_2} = \frac{N_i \cdot w_i \cdot C_i}{\mathcal{L}_i \cdot \epsilon_{\mathrm{vertex}_i} \cdot \Delta M_{\mathrm{JJ}} \cdot \Delta\eta_1 \cdot \Delta\eta_2} \tag{5}$$

where N_i is the number of events in a mass bin, C_i is the unsmearing correction, $\mathcal{L}_i$ is the integrated luminosity, $\epsilon_{\mathrm{vertex}_i}$ is the vertex efficiency, ΔM_{JJ} is the width of the mass bin and $\Delta\eta_{1,2}$ is the width of the eta bin for jets 1 and 2. The cross section is calculated for the pseudorapidity range $|\eta_{1,2}| < 1.0$ in contiguous mass ranges 200, 270, 350 and 550 GeV corresponding to the various software jet thresholds. The final observed cross section corrected for jet and event selection efficiency is shown in Fig. 3. The combined systematic errors are also shown in Fig. 3, ranging from $\sim 10\%$ at 200 GeV to $\sim 20-25\%$ at 850 GeV. The systematic error is dominated by the uncertainty due to the energy scale with smaller contributions due to the unsmearing ($\sim 0.5\% - 2.5\%$), jet selection (1%), vertex selection (1%), vertex cut (1%), and the luminosity matching (5.4% and 2.8% for software thresholds of 30 and 50 GeV). The luminosity scale uncertainty (6.6%) has not been added to the systematic error. The data are plotted at the mass weighted average of the fit function for each bin ($M_{\mathrm{center}} = \int MF(M)dM / \int F(M)dM$).

Figure 3 also shows a prediction for the inclusive dijet mass spectrum from the NLO parton event generator JETRAD [1]. There is good agreement between the prediction and the data over five orders of magnitude. The data and theoretical calculation are binned

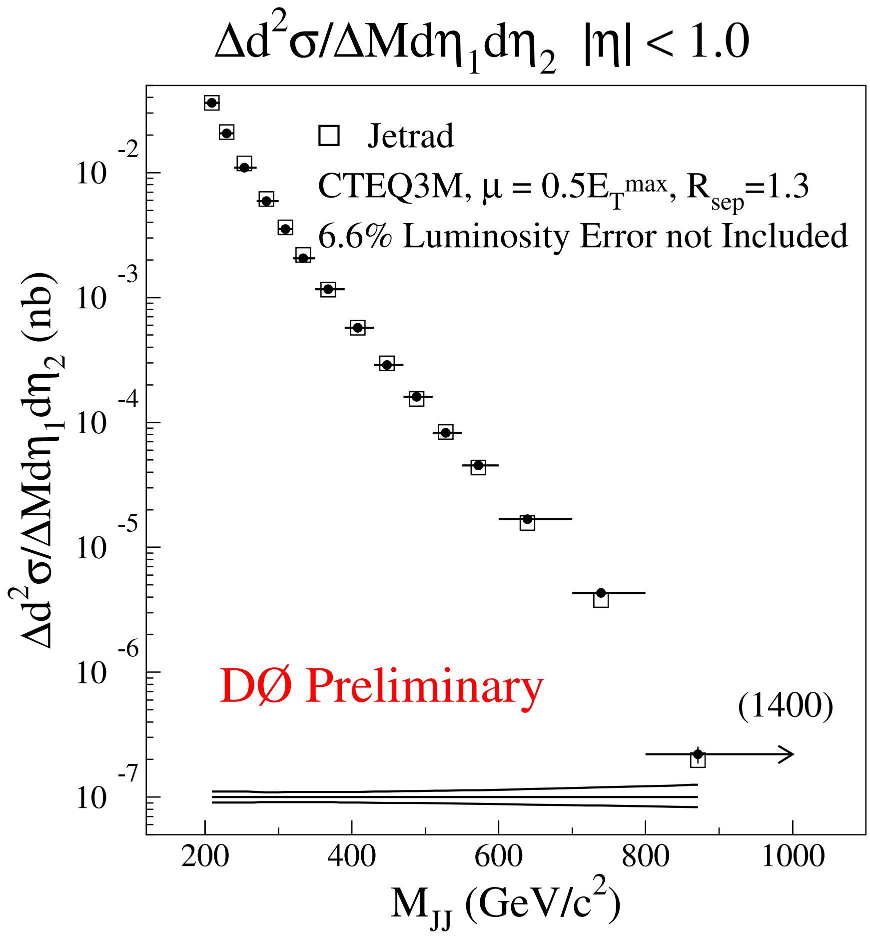

FIG. 3. $\Delta d^2\sigma/\Delta M_{\rm JJ} d\eta_1 d\eta_2$ for $|\eta_{1,2}| < 1.0$ (solid circles). The solid curves represent the plus and minus 1σ systematic errors (excluding the 6.6% luminosity error). The last point represents a mass bin with a range of 800 to 1400 GeV. Also shown is the NLO JETRAD prediction (open squares).

identically in $M_{\rm JJ}$ bins. The NLO calculation requires specification of the renormalization and factorization scale ($\mu = 0.5 \times E_{\rm T}{}^{\rm max}$ where $E_{\rm T}$ is the maximum jet $E_{\rm T}$ in the generated event), parton distribution function (PDF) (CTEQ3M [10]), and a parton clustering algorithm. Partons within 1.3 $\mathcal{R}$ of one another were clustered if they were also within $\mathcal{R}$=0.7 of their $E_{\rm T}$ weighted η, ϕ centroid. The value of 1.3 $\mathcal{R}$ was determined by overlaying jets in data from separate events and determining the separation at which the jet reconstruction algorithm could resolve the individual jets. Variation of the PDF (CTEQ4M, CTEQHJ [11] and MRSA′ [12]) can alter the prediction by up to 30% depending on $M_{\rm JJ}$. Variation of μ between $0.25E_T^{\rm max}$ to $2E_T^{\rm max}$ can alter the predictions normalization by up to 30% with some $M_{\rm JJ}$ dependence. An alternative renormalization scale choice is the center of mass of the interacting partons ($\mu = A\sqrt{\hat{s}} = A\sqrt{x_1 x_2 S}$) which results in a shift of 20% with $M_{\rm JJ}$ dependence for $A = 0.25 - 1.0$.

Figure 4(a) shows the ratio (Data - Theory) / Theory for the JETRAD prediction based on the CTEQ3M PDF. Given the experimental and theoretical uncertainties the prediction is in excellent agreement with the data. Figures 4(b-d) show the effect of varying the choice of renormalization scale and PDF.

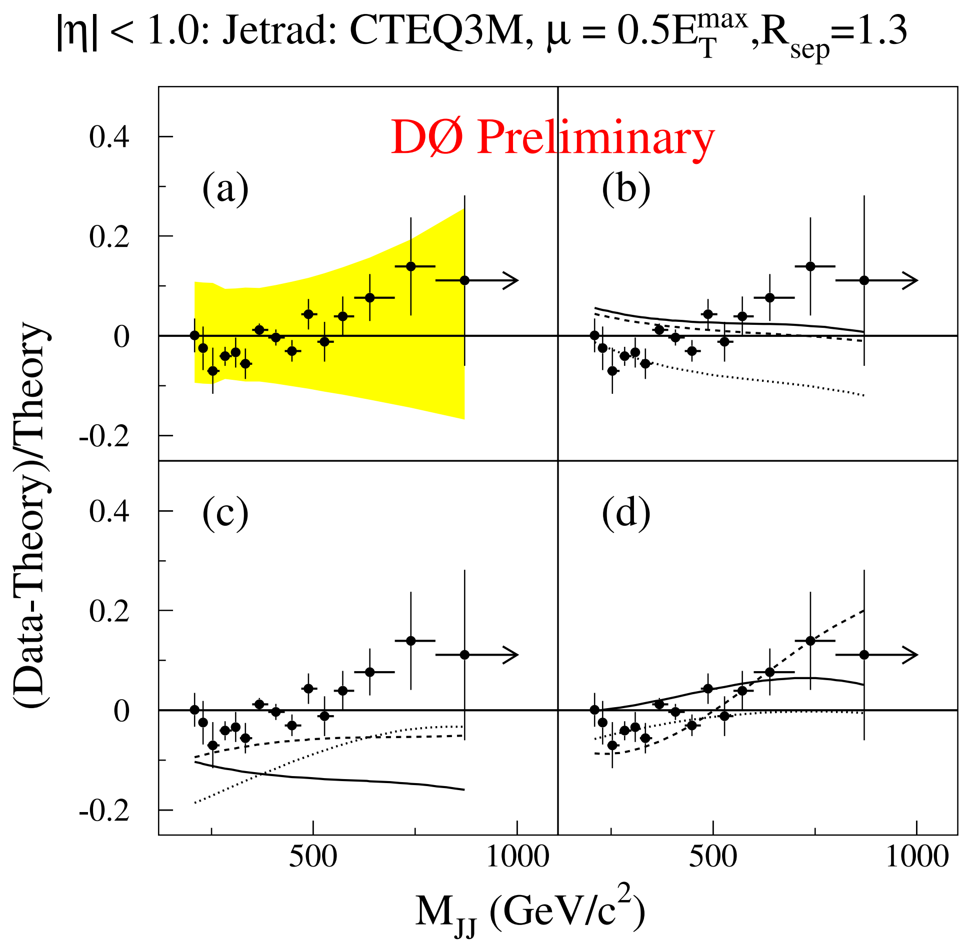

FIG. 4. The difference between the data and the JETRAD prediction divided by the theoretical prediction. The points represent the calculation using the CTEQ3M PDF. (a) The shaded region show the plus and minus 1σ systematic errors (excluding the 6.6% luminosity error). (b) The effect of changing the renormalization scale is shown: $\mu = 0.75 \times E_T^{\max}$ (solid curve), $1.0 \times E_T^{\max}$ (dashed curve) and $2.0 \times E_T^{\max}$ (dotted curve). Note that the theory curve for $\mu = 0.25 \times E_T^{\max}$ cannot be plotted on this scale. (c) $\mu = 1.0 \times \sqrt{x_1 x_2 s}$ (solid curve), $0.5 \times \sqrt{x_1 x_2 s}$ (dashed curve) and $0.25 \times \sqrt{x_1 x_2 s}$ (dotted curve). (d) The effect of choosing a different PDF: MRSA′ (solid curve), CTEQ4HJ (dashed curve) and CTEQ4M (dotted curve).

To examine the inclusive dijet cross section more closely, the data are separated into two rapidity regions: $|\eta_{1,2}| < 0.5$ and $0.5 < |\eta_{1,2}| < 1.0$. The (Data - Theory)/ Data ratio is plotted for these pseudorapidity ranges in Fig 5(a) and (b). In both of these ranges, the data and the JETRAD prediction show similar agreement. The data in the pseudorapidity range $0.5 < |\eta_{1,2}| < 1.0$ is further divided into two samples. The first contains events where the jets have pseudorapidities of opposite sign (OS) and the second sample contains events where the jets have same sign pseudorapidities (SS). Figure 5(c) shows the $0.5 < |\eta_{1,2}| < 1.0$ OS data/theory comparison which shows the same trends as the $0.5 < |\eta_{1,2}| < 1.0$ data. Figure 5(d) shows the comparison for $0.5 < |\eta_{1,2}| < 1.0$ SS. Here the (Data-Theory)/Theory plot shows a different trend to that of the other data sets. However these differences are within the systematic uncertainties.

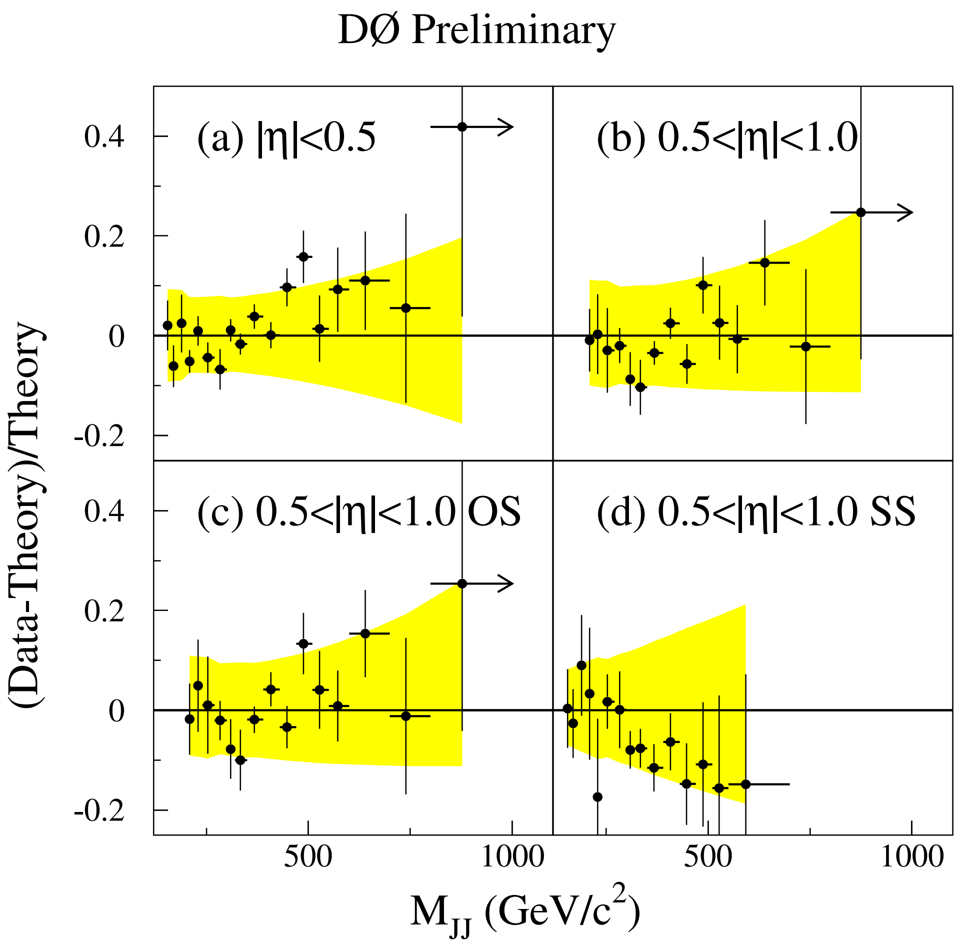

FIG. 5. The difference between the data and the JETRAD prediction divided by the theoretical prediction. The points represent the calculation using the CTEQ3M PDF. The shaded region show the plus and minus 1σ systematic errors (excluding the 6.6% luminosity error) (a) $|\eta_{1,2}| < 0.5$, (b) $0.5 < |\eta_{1,2}| < 1.0$, (c) $0.5 < |\eta_{1,2}| < 1.0$ OS and (d) $0.5 < |\eta_{1,2}| < 1.0$ SS.

VI. CONCLUSION

This analysis is still in progress; it will be finished when the calculation of the correlations in the systematic uncertainties as a function of M_{JJ} are completed.

In conclusion, we have measured the inclusive dijet mass spectrum for a pseudorapidity range of $|\eta_{1,2}| < 1.0$ and $200 < M_{JJ} < 1400$ GeV at $\sqrt{s} = 1.8$ TeV. The QCD NLO model, using three different PDF's is in excellent agreement with the shape of the observed inclusive dijet mass spectrum.

ACKNOWLEDGEMENTS

We thank the staffs at Fermilab and collaborating institutions for their contributions to this work, and acknowledge support from the Department of Energy and National Science Foundation (U.S.A.), Commissariat à L'Energie Atomique (France), State Committee for Science and Technology and Ministry for Atomic Energy (Russia), CNPq (Brazil), Departments of Atomic Energy and Science and Education (India), Colciencias (Colombia), CONACyT (Mexico), Ministry of Education and KOSEF (Korea), and CONICET and UBACyT (Argentina).

REFERENCES

* Visitor from IHEP, Beijing, China.

† Visitor from Universidad San Francisco de Quito, Quito, Ecuador.

[1] W.T. Giele, E.W.N. Glover and D.A. Kosower, *Higher Order Corrections to Jet Cross Sections in Hadron Collisions*, Nucl. Phys. **B403**, 633 (1993).

[2] S.D. Ellis, Z. Kunszt and D.E. Soper, *The One Jet Inclusive Cross-Section at Order* ${\alpha_s}^2$ *Quarks and Gluons*, Phys. Rev. Lett. **64**, 2121 (1990).
Z Kunszt and D.E. Soper *Calculation of Jet Cross-Sections in Hadron Collisions at Order* ${\alpha_s}^2$, Phys. Rev. **D46**, 192 (1992).

[3] F. Aversa, et al., Phys. Rev. Lett. **65**, (1990)

[4] DØ Collaboration, S. Abachi *et al.*, Nucl. Instrum. Methods **A338**, 185 (1994).

[5] S. Abachi et al., (DØ Collaboration), Phys. Lett. **B257**, 232 (1995)

[6] D. Elvira, *Measurement of the Inclusive Jet Cross Sections at* $\sqrt{s} = 1.8\,TeV$ *with the DØ Detector*, Ph.D. Thesis, (1993)

[7] R. Kehoe (for the DØ Collaboration) *Hadronic Calibration of DØ Calorimetry*, Submitted to the International Conference on Calorimetry in High Energy Physics, Laboratori Nazionali di Franscati, Frascati, Italy, Jun 8-14, 1996, FERMILAB-CONF-96-284-E.

[8] Particle Data Group, "Review of Particle Properties", Phys. Rev D**50**, 1336 (1994).

[9] H.U. Bengtsson and T. Sjöstrand, Computer Physics Commun. **46** (1987) 43.

[10] By: H.L. Lai et al., *Global QCD Analysis and the CTEQ Parton Distributions*, Phys. Rev. **D51**, 4763 (1995).

[11] By: H.L. Lai et al., *Improved Parton Distributions from Global Analysis of Recent Deep Inelastic Scattering and Inclusive Jet Data*, Phys. Rev. **D55**, 1280 (1997).

[12] A.D. Martin, R.G. Roberts and W.J. Stirling, Phys. Lett. **B354**, 154 (1995).